Vickers hardness and compressive properties of bulk metallic glasses and nanostructure-dendrite composites

X.F. Pan
Shenyang National Laboratory for Materials Science, Institute of Metal Research, Chinese Academy of Sciences, Shenyang 110016, People's Republic of China; and School of Materials Science and Engineering, Tianjin University, Tianjin 300072, People's Republic of China

H. Zhang and Z.F. Zhang[a)]
Shenyang National Laboratory for Materials Science, Institute of Metal Research, Chinese Academy of Sciences, Shenyang 110016, People's Republic of China

M. Stoica
Leibniz Institute for Solid State and Materials Research Dresden, Institute of Metallic Materials, D-01171 Dresden, Germany

G. He
School of Materials Science and Engineering, Shanghai Jiaotong University, Shanghai 200030, People's Republic of China

J. Eckert[b)]
Physical Metallurgy Division, Department of Materials and Geo Sciences, Darmstadt University of Technology, D-64287 Darmstadt, Germany

(Received 4 February 2005; accepted 14 April 2005)

The compressive properties and the Vickers hardness of Cu-, Fe-, Mg-, and Zr-based monolithic bulk metallic glasses (BMGs) as well as Ti-based nanostructure-dendrite composites were investigated and compared. The monolithic BMGs exhibit nearly the same yield strength σ_y and fracture strength σ_f but poor plasticity. The Vickers hardness H_V of the monolithic BMGs follows the empirical relationship $H_V/3 \approx \sigma_y \approx \sigma_f$. The Ti-based composites yield at a relatively low stress level (less than 850 MPa) but fail at a very high fracture stress (~2 GPa) and exhibit a large strain hardening ability. Accordingly, the Vickers hardness H_V of the Ti-based nanostructure-dendrite composites obeys the relationship $\sigma_y < H_V/3 < \sigma_f$. Based on these results, the relationship between the Vickers hardness and the compressive properties of the investigated materials will be discussed by taking the yield and fracture strength (σ_y and σ_f), the strain hardening exponent n, and the elastic and plastic energy stored upon deformation (δ_E and δ_P) into account.

I. INTRODUCTION

In 1960, an Au–Si metallic alloy with amorphous structure was first discovered.[1] After that, many attempts have been devoted to amorphization of a variety of alloys.[2–4] Finally, starting at the at the beginning of the 1990s and continuing since then, Zr-, Cu-, and Pd-based bulk metallic glasses and also other classes of easy glass-forming alloys were discovered and successfully fabricated.[5–7] A large amount of investigations in the recent decade has demonstrated that bulk metallic glasses (BMGs) possess novel physical, chemical, and mechanical properties and have a large potential for a variety applications,[8–10] which has created extensive interest among scientists and engineers. Normally, metallic materials with glassy structure exhibit very high strength and hardness value, a relatively low Young's modulus, and almost perfect elastic-plastic behavior upon room temperature deformation.[11,12] Therefore, the discovery of BMGs opens up new opportunities to reveal the basic deformation and fracture mechanisms of matter.[13]

In addition to monolithic metallic glasses, in situ formed Zr- and Ti-based metallic glass matrix composites with ductile dendritic precipitates as well as nanostructure/dendrite composites have recently been obtained, which

a)Address all correspondence to this author.
e-mail: zhfzhang@imr.ac.cn
b)This author was an editor of this journal during the review and decision stage. For the *JMR* policy on review and publication of manuscripts authored by editors, please refer to http://www.mrs.org/publications/jmr/policy.html.
DOI: 10.1557/JMR.2005.0328

exhibit a dramatic increase in plastic deformability under quasi-static compression.[14–18] The enhanced ductility of such composites is attributed to the blocking effects of the dendrites dispersed in the matrix, acting as obstacles hindering the propagation of shear bands.[14,15,17–20]

Compressive testing and Vickers hardness measurements are two typical and convenient methods for revealing the deformation and fracture mechanisms of BMG materials. By employing these techniques, one can easily measure the yield and fracture strength (σ_y and σ_f), the ductility, Young's modulus, and the hardness of the materials. A large amount of investigations have shown that there is an empirical relationship, i.e. $\sigma_f \approx H_V/3$,[21] between the fracture strength σ_f and the Vickers hardness H_V of monolithic bulk metallic glasses.[22–29] However, so far there is no report about such a relationship for BMGs or nanostructured composites containing ductile dendrites. In this work, we investigated a series of metallic glasses with a wide range of fracture strength and Young's modulus and compare the data with the results obtained for Ti-based nanostructure-dendrite composites. The main purpose of this work is to reveal the factors affecting the hardness of the materials by taking their compressive properties into account.

II. EXPERIMENTAL PROCEDURE

Five different metallic glassy alloys or nanostructure-dendrite composites were used for the current investigations, i.e., (i) monolithic metallic glasses, including $Mg_{65}Cu_{7.5}Ni_{7.5}Zn_5Ag_5Y_{10}$, $Zr_{59}Cu_{20}Al_{10}Ni_8Ti_3$, $Cu_{60}Zr_{30}Ti_{10}$, and $Fe_{65.5}Cr_4Mo_4Ga_4P_{12}C_5B_{5.5}$, and (ii) $Ti_{50}Cu_{22}Ni_{20}Sn_3Si_2B_3$ nanostructured composites with ductile body-centered-cubic (bcc) type dendrites. The monolithic BMGs were prepared by arc melting the mixture of the pure elements in a Ti-gettered argon atmosphere to obtain master ingots. These master ingots were then remelted several times to ensure the homogeneity. To prepare the $Ti_{50}Cu_{22}Ni_{20}Sn_3Si_2B_3$ composites, one method was to cast the master alloy ingots into a copper mold of dimensions Φ 3 × 100 mm. Alternatively, the composites were prepared by arc-melting the master alloy ingots several times and cooling on the copper hearth at a slower rate. The $Ti_{50}Cu_{22}Ni_{20}Sn_3Si_2B_3$ composites fabricated by both arc-melting and casting consisted of a nanostructured matrix and ductile bcc-type dendritic precipitates.[30] The details of the fabrication processes of the BMGs and the nanostructure-dendrite composites have already been described elsewhere.[17,18,30–33]

The Vickers hardness was measured using a MVK-H3 Vickers microhardness tester. For these measurements, the specimen surfaces were carefully polished before testing. The tests were preformed using a typical diamond indenter in the form of pyramid with square base and an angle of 136° between opposite faces. A load of 4.9 N was applied for 10 s. The diagonal of the indentation as well as the hardness was calculated using a digital video measuring system.

Two kinds of samples, i.e., rectangular bars with dimensions of 3 × 3 × 6 mm or rods with dimensions of Φ 3 × 6 mm, were machined from the as-solidified specimens for compression testing. The tests were performed using a MTS810 test system at a strain rate of 10^{-4} s^{-1} at room temperature. From the compression stress–strain curves, the yield strength σ_y, the yield strain ε_y, the fracture strength σ_f, the fracture strain ε_f, and Young's modulus E were derived. To investigate the effects of indentation on the formation of the shear bands, the Vickers hardness tester was used to induce a series of indentations on the polished surfaces of some of the samples before compression testing. The characteristics of the fracture surfaces as well as the features of the indents after the hardness tests were studied by using a Cambridge S360 scanning electron microscope (SEM).

III. RESULTS AND DISCUSSION

Figure 1 shows the room-temperature compressive stress–strain curves of all the BMGs and the Ti-based composites. The mechanical properties of all the samples (A–F) are listed in Table I. It can be seen that the fracture strength σ_f of the different alloys spans over a wide range of 851–2840 MPa; Young's modulus E also varies greatly between 49 and 161 GPa, as shown in Table I. The plastic strain at failure for the monolithic metallic glass samples A, D, E, and F is less than 1.0%, but the Ti-based composites exhibit a relatively high ductility of 4.4% (B) or 11.5% (C), respectively. Another feature is that the yield strength σ_y of all the monolithic metallic glasses is quite close to the fracture strength σ_f, indicating that there is no obvious strain hardening before

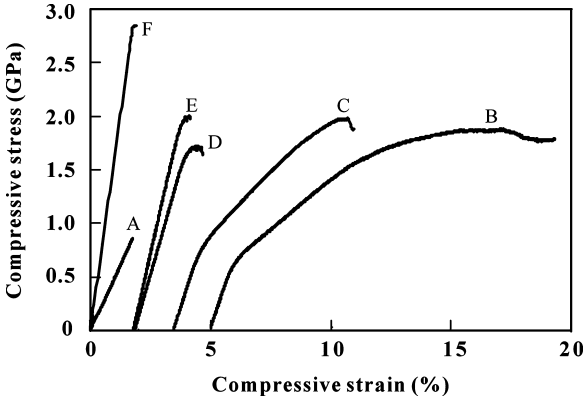

FIG. 1. Compressive stress–strain curves of samples A–F: (A) $Mg_{65}Cu_{7.5}Ni_{7.5}Zn_5Ag_5Y_{10}$, (B) $Ti_{50}Cu_{22}Ni_{20}Sn_3Si_2B_3$ (as-arc-melted), (C) $Ti_{50}Cu_{22}Ni_{20}Sn_3Si_2B_3$ (as-cast), (D) $Zr_{59}Cu_{20}Al_{10}Ni_8Ti_3$, (E) $Cu_{60}Zr_{30}Ti_{10}$, and (F) $Fe_{65.5}Cr_4Mo_4Ga_4P_{12}C_5B_{5.5}$.

TABLE I. Mechanical properties of the monolithic metallic glasses and the Ti-based composites with dendritic phases.

Sample	Metallic glasses	σ_y (MPa)	ϵ_y (%)	σ_f (MPa)	ϵ_p (%)	E (GPa)	H_v (GPa)	δ_E (MJ/m^3)	δ_T (MJ/m^3) (%)	δ_E/δ_T	δ_P/δ_T (%)
A	$Mg_{65}Cu_{7.5}Ni_{7.5}Zn_5Ag_5Y_{10}$	851	1.76	851	0	49	2.35	7.37	7.37	100	0
B	$Ti_{50}Cu_{22}Ni_{20}Sn_3Si_2B_3$ (arc-melting)	647	2.9	1880	11.5	68	3.44	25.99	155.3	17.3	82.7
C	$Ti_{50}Cu_{22}Ni_{20}Sn_3Si_2B_3$ (as-cast)	817	2.0	1970	4.4	70	4.38	27.72	69.4	40.1	59.9
D	$Zr_{59}Cu_{20}Al_{10}Ni_8Ti_3$	1610	1.0	1710	0.8	78	4.69	18.74	29.81	62	38
E	$Cu_{60}Zr_{30}Ti_{10}$	1720	1.9	2010	0.4	99	5.78	20.16	27.14	74.3	25.7
F	$Fe_{65.5}Cr_4Mo_4Ga_4P_{12}C_5B_{5.5}$	2820	1.76	2840	0.15	161	8.67	25.05	28.5	87.9	12.1

failure. The yield strength of the Ti-based composites B and C are 647 and 817 MPa. These alloys display a pronounced strain-hardening ability, and their final fracture strength reaches values of 1880 MPa (B) or 1970 MPa (C), respectively.

The fracture surface features of the $Zr_{59}Cu_{20}Al_{10}Ni_8Ti_3$ monolithic metallic glass and of the as arc-melted $Ti_{50}Cu_{22}Ni_{20}Sn_3Si_2B_3$ composite are shown in Fig. 2. For the fully amorphous alloy, failure occurs in a shear mode, and the shear fracture surface makes an angle of approximately 43° with respect to the compression axis.[31] The shear fracture surface exhibits typical veinlike patterns [Figs. 2(a) and 2(b)], as reported also for different metallic glasses.[12,24,28,31,34,35] A similar fracture feature was also observed in A, D, E, and F monolithic BMG samples. The fracture surface of the arc-melted Ti-based composite sample (B) displays a relatively rough feature in comparison with the fully amorphous alloys [Fig. 2(c)]. The rough fracture surface of the composite can be attributed to the strong interactions between shear bands and the dendrites, resulting in a high ductility.[19,20] The typical shear fracture surfaces of the composites still contain veinlike features, as displayed in Fig. 2(d), indicating the occurrence of melting during shear fracture.

Figure 3(a) shows the dependence of Vickers hardness H_V on the applied load for $Zr_{59}Cu_{20}Al_{10}Ni_8Ti_3$ (D) and $Ti_{50}Cu_{22}Ni_{20}Sn_3Si_2B_3$ (B) samples, respectively. It can be seen that the hardness decreases with increasing the applied load P. When the applied load is higher than 1 N, the hardness approximately remains constant. These results for the metallic glasses are similar to the experimental results reported by Li et al.[36] They found that the indenter/specimen interfacial friction in Vickers indentation testing has a minimal effect in the high load regime whereas it has a significant effect in the low load regime. Therefore, a load in the range of 1–10 N, i.e., 4.9 N was selected for the current hardness tests.

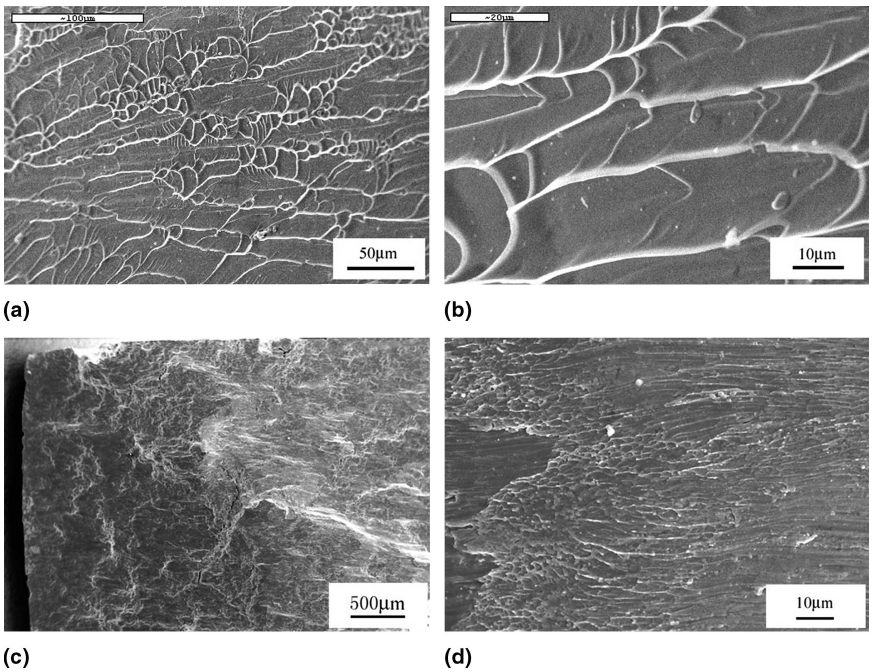

FIG. 2. Typical fracture surface features of some metallic glasses: (a, b) $Zr_{59}Cu_{20}Al_{10}Ni_8Ti_3$ and (c, d) $Ti_{50}Cu_{22}Ni_{20}Sn_3Si_2B_3$ (as-arc-melted).

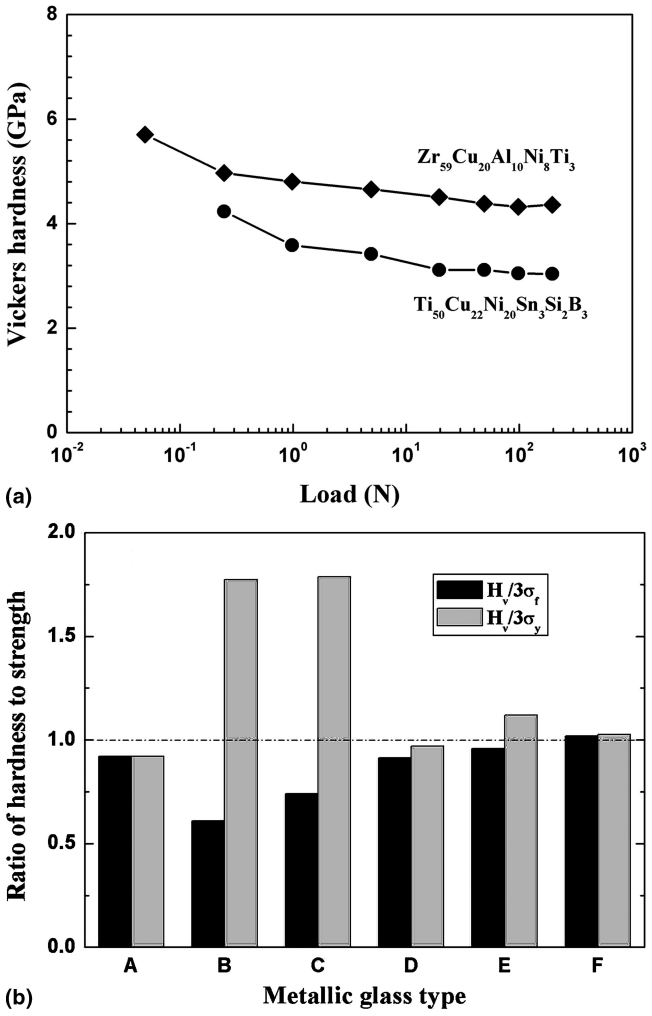

FIG. 3. (a) H_V-P curves of samples C and D; (b) relationship between $H_V/3$ and σ_f (σ_y) for samples A–F.

The hardness values for all the samples studied here increase in the order of A–F from 2.35 to 8.67 GPa, as listed in Table I. For all the monolithic BMGs, their yield strength and fracture strength are almost the same. Therefore, the ratios of $H_V/3\sigma_f$ or $H_V/3\sigma_y$ are quite close to 1, as seen in Fig. 3(b). This indicates that the hardness of the monolithic metallic glasses (A, D, E and F) follows the empirical relationship $H_V/3 \approx \sigma_f$.[21] For the two Ti-based composites (B and C), their ratios of $H_V/3\sigma_f$ are equal to 0.6 and 0.74; however, the ratios of $H_V/3\sigma_f$ are 1.77 and 1.78, respectively. This reveals that the hardness and the strength of the Ti-based composites do not follow the relationship $\sigma_f \approx H_V/3$. For comparison, some data of strength and hardness for ultra-fine-grained Al and nanocrystalline Cu and Ni samples are summarized in Table II.[37] It can be clearly seen that both H_V/σ_y and H_V/σ_f are far from 3 for the three materials with relatively high strength, indicating that the empirical relationship is also invalid for those nanocrystalline materials.

The dependences of the hardness H_V on the Young's modulus E and the yield or fracture strength (σ_y or σ_f) for various metallic glasses available[22–29] are shown in Figs. 4(a) and 4(b). The data for the BMGs investigated in our study are also plotted in Figs. 4(a) and 4(b) for comparison. First, H_V follows an approximately linear relationship with Young's modulus E for a large number of metallic glasses over a wide range of E, as shown in Fig. 4(a). This indicates that the hardness H_V is proportional to the Young's modulus E for a variety of metallic glasses.[22–29] Secondly, the hardness of all the monolithic BMGs follows the relationship $\sigma_f \approx H_V/3$ because their yield and fracture strength are nearly the same, as shown in Fig. 4(b). Since the Ti-based composites B and C exhibit higher ductility and strong strain hardening, their yield and fracture strength have a great difference. Therefore, the ratios of H_V/σ_y or H_V/σ_f for the Ti-based composites B and C always deviate from the trend line in Fig. 4(b). This gives rise to the question of what is the major factor affecting the hardness of the Ti-based composites in the regime between the yield and the fracture strength. This issue will be discussed below.

The SEM micrographs of the indentations on the surfaces of the samples C and D before and after compression testing are shown in Fig. 5. For the monolithic metallic glass D, "coronet" shear bands are observed at the edge of the indentation put down before the compression test [Fig. 5(a)]. The newly formed shear bands introduced during compression pass through the indentation and the "coronet" shear bands. However, the shape and propagation direction of the initial shear bands introduced by indentation do not change after compression [Fig. 5(b)]. Also the indentations on the surfaces of the as-cast Ti-based composite (C) maintain the same shape after the compressive test [see Figs. 5(c) and 5(d)]. This indicates that the existing indentations on the surfaces of both the monolithic BMGs and the Ti-based composites do no affect the formation and development of the new shear bands introduced upon compression.

TABLE II. Relationship between tensile strength and hardness of some nano-materials.[36]

Materials	Grain size (nm)	Yield strength σ_y (MPa)	Fracture strength σ_f (MPa)	Hardness (GPa)	H_v/σ_y	H_v/σ_f
Ultra-fine-grained Al	250	135	220	1.0	7.4	4.5
Nano-Cu	26	535	880	2.4	4.5	2.7
Nano-Ni	28	1150	1550	4.8	4.2	3.1

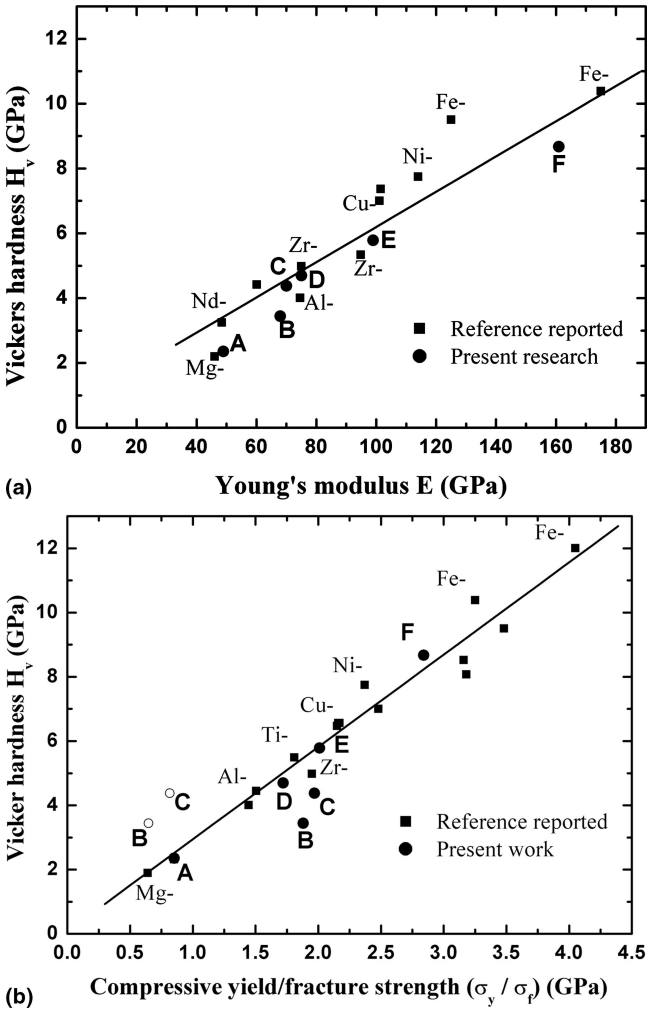

FIG. 4. (a) H_V-E and (b) H_V-σ_y (○) or H_V-σ_f (●) relationship of samples A–F and other metallic glasses available.

In general, the hardness reflects the resistance of a material to deformation. The final indentation size is a measurement of the resistance of the material against permanent (plastic) deformation. Therefore, the hardness can be affected by the shape of indentation, the applied load, the strain hardening exponent n, and other material properties.[38] As mentioned above, there is an empirical relationship between the fracture stress and the hardness, i.e., $\sigma_f \approx H_V/3$.[21] Normally, monolithic metallic glasses obey this relationship well; however, there is a significant deviation for the Ti-based composites with larger ductility, as shown in Fig. 3(b).

For a better understanding of the hardness and the compressive properties of the BMGs and the Ti-based composites, the stress–strain curves of samples B, C, and E are schematically illustrated in Fig. 6 because the three samples have approximately the same fracture strength of ~2.0 GPa. However, their Vickers hardness are 3.4 GPa (B), 4.4 GPa (C), and 5.8 GPa (E), respectively. In addition, the yield strength of these samples are equal to 647 MPa (B), 817 MPa (C), and 1720 MPa (E), respectively. It seems that the material with higher yield strength has a higher hardness. For the Ti-based composites, their hardness follows the relationship $\sigma_y < H_V/3 < \sigma_f$. This indicates that the hardness of these materials with strong strain-hardening ability is not only affected by the fracture strength σ_f, but also by the yield strength σ_y. For simplicity, it is assumed that the hardness H_V of such materials can be expressed as a function of the yield strength σ_y and the fracture strength σ_f, i.e.,

$$H_V/3_V = x\sigma_y + (1 - x)\sigma_f \ (0 < x < 1) \quad , \qquad (1)$$

where x represents the contribution of yield strength σ_y to the hardness, and $(1 - x)$ reflects the contribution of fracture strength σ_f to the hardness. In the present study, the values of x_B and x_C for the samples B and C are 0.59 and 0.44, respectively, as calculated by Eq. (1) and the data in Table I. This indicates that the yield strength plays a more important role in the hardness for sample B than for sample C. In addition, the strain hardening exponent n represents the hardening rate of a material after yielding. Therefore, the strain hardening exponent n of the samples B and C was calculated from their stress–strain curves in Fig. 1. The calculated strain hardening exponents n of the samples B and C are 0.5 and 0.54, respectively. This means that the hardness of the samples with strong strain hardening ability will be higher although they have nearly the same fracture strength σ_f. Therefore, the strain hardening exponent n is also one of the factors affecting the hardness of the materials.

During the compression testing, the total applied energy can be transformed into elastic and plastic energy. The hardness of a material represents its ability to resist permanent plastic deformation. Therefore, the elastic and plastic energy absorbed by a compressed sample should be considered. The normal elastic energy density δ_E at failure is given by the shadowed area as illustrated in Fig. 6, and the total energy density δ_T is defined as the area below the stress-strain curve. Hence, the difference between δ_T and δ_E is the plastic energy density δ_P, and δ_T, δ_E as well as δ_P can be expressed as

$$\delta_T = \int_0^{\epsilon_f} \sigma d\epsilon \quad , \qquad (2)$$

$$\delta_E = \sigma_f^2/2E \quad , \qquad (3)$$

$$\delta_P = \delta_T - \delta_E \quad . \qquad (4)$$

The values of δ_E and δ_T as well as the ratios of δ_E to δ_T and δ_P to δ_T were calculated by Eqs. (2)–(4), and are listed in Table I. For the investigated BMG materials, when δ_E/δ_T is larger, the corresponding hardness is

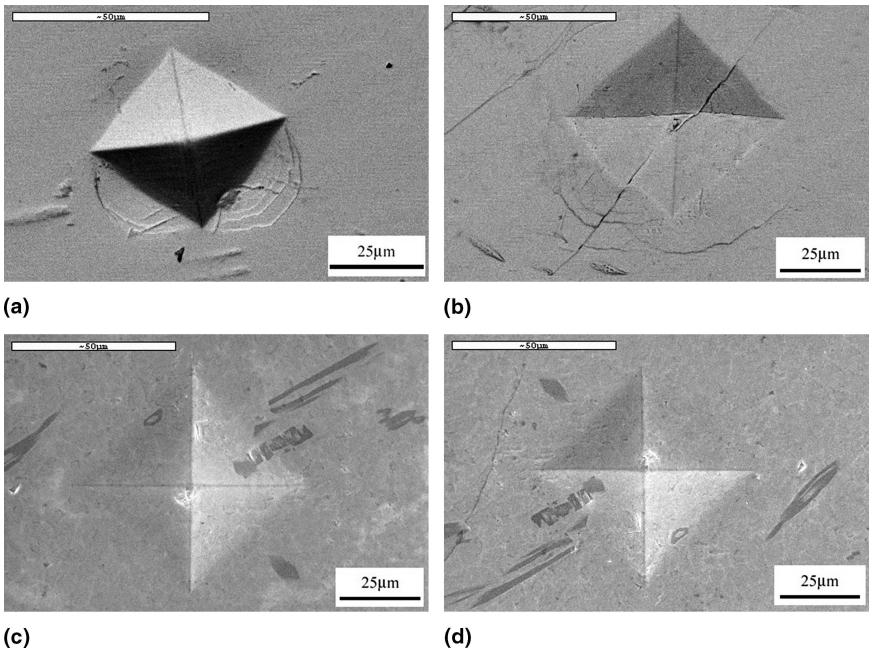

FIG. 5. Typical micrograph of indentation: (a, b) the indentations of sample D before and after compressive testing and (c, d) the indentations of sample C before and after compressive testing.

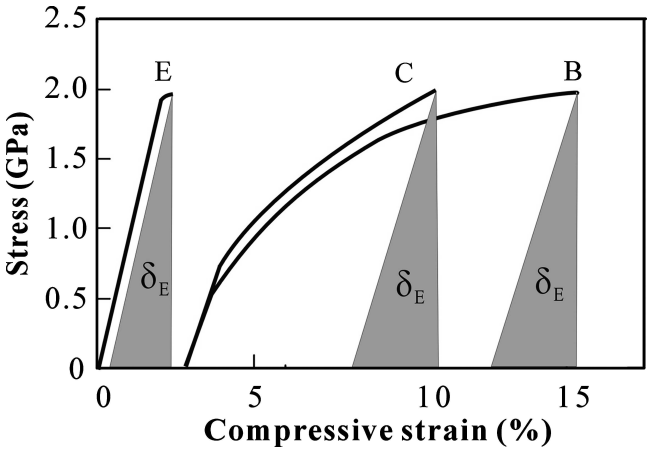

FIG. 6. Schematic illustration of stress–strain curves of samples B, C, and E.

higher. It seems that the relative magnitudes of δ_P/δ_T and δ_E/δ_T during the deformation process can also affect the hardness of the Ti-based composites. The hardness will increase with increasing δ_E/δ_T for samples B, C, D, E, and F. When δ_E/δ_T is higher, the applied energy related to the plastic deformation is smaller. Thus, the ability of the materials resisting permanent deformation is relatively stronger, resulting in a higher hardness. This might be one of reasons why the hardness of samples B, C, D, E, and F increases with increasing value of δ_E/δ_T, if not considering the atomic bonding properties of different composites in the materials above.

From the above discussion, the monolithic metallic glasses were found to obey the well-known empirical relationship $H_V/3 \approx \sigma_f$. However, the deformation of the Ti-based composites with larger ductility deviates from this relationship. It can be concluded that the hardness of all the BMGs and their composites cannot simply be expressed as $H_V/3 \approx \sigma_f$, but other compressive properties, such as σ_f, σ_y, E, n, and δ_E/δ_T also play significant roles in determining the hardness. Therefore, one can assume that the hardness of a material should be a function of these properties, i.e.,

$$H_V/3 = \sigma_y + f(\sigma_f, E, \delta_E, \delta_T, n) \quad . \tag{5}$$

However, the detailed relationship between these parameters is not clear yet, but needs further investigation.

IV. CONCLUSIONS

The monolithic metallic glasses materials exhibit high yield and fracture strength, but poor ductility. Their hardness H_V follows the empirical relationship $H_V/3 \approx \sigma_f \approx \sigma_y$.

The Ti-based nanostructure-dendrite composites exhibit a high fracture strength (~2.0 GPa) and distinct ductility in contrast to the monolithic metallic glasses. They yield at a relatively low stress level (less than 850 MPa) and display a strong strain-hardening ability. Their hardness H_V follows the relationship $\sigma_y < H_V/3 < \sigma_f$. Accordingly, the hardness of such materials is not only affected by the fracture strength, but also by yield strength.

The elastic energy δ_E and the plastic energy δ_P represent the ability of a material to resist the elastic and plastic deformation. The contribution of the elastic and plastic energy δ_E and δ_P may also affect the hardness of

a material. When δ_E / δ_T increases, the contribution of the applied energy to the plastic deformation is smaller. As a result, the ability of the material to resist plastic deformation is higher, resulting in a high hardness.

ACKNOWLEDGMENTS

The authors thank H.H. Su, J.L. Wen, G. Yao, X. Shi, Y.K. Xu, and J. Xu for technical assistance and stimulating discussions. This work was supported by the National Natural Science Funds of China (NSFC) under Grants No. 50401019 and 50323009, and the "Hundreds of Talents Project" by the Chinese Academy of Sciences. M.S. and J.E. are grateful for the financial support from the German Science Foundation under Grant No. Ec 111/12-1 and from the EU within the framework of the RTN-networks on bulk metallic glasses (HPRN-CT-2000-00033) and ductile BMG composites (MRTN-CT-2003-504692).

REFERENCES

1. J.W. Klement, R.H. Willens, and P. Duwez: Non-crystalline structure in solidified gold-silicon. *Nature* **187,** 869 (1960).
2. A.S. Argon: Plastic deformation in metallic glasses. *Acta Metall.* **27,** 47 (1979).
3. V.Z. Bengusc, P. Diko, K. Csach, J. Miskuf, V. Ocelik, E.B. Korolkova, E.D. Tabachnikova, and P. Duhaj: Failure crack orientation at ductile shear fracture of $Fe_{80-x}Ni_xB_{20}$ metallic glass ribbons. *J. Mater. Sci.* **25,** 1598 (1990).
4. P.E. Donovan: Compressive deformation of amorphous $Pd_{40}Ni_{40}P_{20}$. *Mater. Sci. Eng.* **98,** 487 (1988).
5. A. Inoue, T. Zhang, and T. Masumoto: Zr–Al–Ni amorphous alloys with high glass transition temperature and significant supercooled liquid region. *Mater. Trans. JIM* **31,** 177 (1990).
6. A. Inoue, W. Zhang, T. Zhang, and K. Kurosaka: High-strengtth Cu-based bulk glassy alloys in Cu–Zr–Ti and Cu–Hf–Ti ternary systems. *Acta Mater.* **49,** 2645 (2001).
7. P. De Hey, J. Sietsma, and A. van den Beukel: Structural disordering in amorphous $Pd_{40}Ni_{40}P_{20}$ induced by high temperature deformation. *Acta Mater.* **46,** 5873 (1998).
8. W.L. Johnson: Bulk glass-forming metallic alloys: Science and technology. *MRS Bull.* **24,** 42 (1999).
9. A. Inoue: Stabilization of metallic supercooled liquid and bulk amorphous alloys. *Acta Mater.* **48,** 279 (2000).
10. W.H. Wang, C. Dong, and C.H. Shek: Bulk metallic glasses. *Mater. Sci. Eng. Rep.* **44,** 45 (2004).
11. C.A. Pampillo: Review: Flow and fracture in amorphous alloys. *J. Mater. Sci.* **10,** 1194 (1975).
12. C.T. Liu, L. Heatherly, D.S. Easton, et al.: Test environment and mechanical properties of Zr-based bulk amorphous alloys. *Metall. Mater. Trans.* **A29,** 1811 (1998).
13. Z.F. Zhang and J. Eckert: Unified tensile fracture criterion. *Phys. Rev. Lett.* **94,** 094301 (2005).
14. C.C. Hays, C.P. Kim, and W.L. Johnson: Microstructure controlled shear band pattern formation and enhanced plasticity of bulk metallic glasses containing in situ formed ductile phase dendrite dispersions. *Phys. Rev. Lett.* **84,** 2901 (2000).
15. F. Szuecs, C.P. Kim, and W.L. Johnson: Mechanical properties of $Zr_{56.2}Ti_{13.8}Nb_{5.0}Cu_{6.9}Ni_{5.6}Be_{12.5}$ ductile phase reinforced bulk metallic glass composite. *Acta Mater.* **49,** 1507 (2001).
16. U. Kühn, J. Eckert, N. Mattern, and L. Schultz: ZrNbCuNiAl bulk metallic glass composites containing dendritic bcc phase precipitates. *Appl. Phys. Lett.* **80,** 2478 (2002).
17. G. He, J. Eckertx, W. Löser, and L. Schultz: Novel Ti-base nanostructure-dendrite composite with enhanced plasticity. *Nat. Mater.* **2,** 33 (2003).
18. G. He, J. Eckert, W. Löser, and M. Hagiwara: Composition dependence of the microstructure and the mechanical properties of nano/ultrafine-structured Ti–Cu–Ni–Sn–Nb alloys. *Acta Mater.* **52,** 3035 (2004).
19. Z.F. Zhang, G. He, H. Zhang, and J. Eckert: Rotation mechanism of shear fracture induced by high plasticity in Ti-based nanostructured composites containing ductile dendrites. *Scripta Mater.* **52,** 945 (2005).
20. H. Zhang, X.F. Pan, Z.F. Zhang, J. Das, K.B. Kim, C. Müller, M. Kusy, A. Gebert, G. He, and J. Eckert: Toughening mechanisms of a Ti-based nanostructured composite containing ductile dendrites. *Z. Metall.* (2005, in press).
21. H.S. Chen: Glassy metals. *Rep. Prog. Phys.* **43,** 533 (1980).
22. S.G. Kim, A. Inoue, and T. Masumoto: High mechanical strength of Mg–Ni–Y and Mg–Cu–Y amorphous alloys with significant supercooled liquid region. *Mater. Trans. JIM.* **31,** 933 (1990).
23. M.L. Vaillant, V. Keryvin, T. Rouxel, and Y. Kawamura: Changes in the mechanical properties of a $Zr_{55}Cu_{30}Al_{10}Ni_5$ bulk metallic glass due to heat treatments below 540°C. *Scripta Mater.* **47,** 19 (2002).
24. A. Inoue, S. Sobu, D.V. Louzguine, H. Kimura, and K. Sasamori: Ultrahigh strength Al-based amorphous alloys containing Sc. *J. Mater. Res.* **19,** 1539 (2004).
25. A. Inoue and W. Zhang: Formation, thermal stability and mechanical properties of Cu–Zr and Cu–Hf binary glassy alloy rods. *Mater. Trans.* **45,** 584 (2004).
26. W. Zhang and A. Inoue: Formation and mechanical properties of Ni-based Ni–Nb–Ti–Hf bulk glassy alloys. *Scripta Mater.* **48,** 641 (2003).
27. A. Inoue, B.L. Shen, A.R. Yavari, and A.L. Greer: Mechanical properties of Fe-based bulk glassy alloys in Fe–B–Si–Nb and Fe–Ga–P–C–B–Si systems. *J. Mater. Res.* **18,** 1487 (2003).
28. A. Inoue, B.L. Shen, and C.T. Chang: Super-high strength of over 4000 MPa for Fe-based bulk glassy alloys in $[(Fe_{1-x}Co_x)_{0:75}B_{0:2}Si_{0:05}]_{96}Nb_4$ system. *Acta Mater.* **52,** 4093 (2004).
29. Y.C. Kim, W.T. Kim, and D.H. Kim: A development of Ti-based bulk metallic glass. *Mater. Sci. Eng.* **A375–377,** 127 (2004).
30. Z.F. Zhang, G. He, and J. Eckert: Shear and distensile fracture behavior of Ti-based composite with ductile dendrites. *Philos. Mag.* **85,** 897 (2005).
31. Z.F. Zhang, J. Eckert, and L. Schultz: Difference in compressive and tensile fracture mechanisms of $Zr_{59}Cu_{20}Al_{10}Ni_8Ti_3$ bulk metallic glass. *Acta Mater.* **51,** 1167 (2003).
32. M. Stoica, J. Eckert, S. Roth, Z.F. Zhang, L. Schultz, and W.H. Wang: Mechanical behavior of $Fe_{65.5}Cr_4Mo_4Ga_4P_{12}C_5B_{5.5}$ bulk metallic glass. *Intermetallics* **13,** 764 (2005).
33. H. Men, Z.Q. Hu, and J. Xu: Bulk metallic glass formation in the Mg–Cu–Zn–Y system. *Scripta Mater.* **46,** 700 (2002).
34. W.J. Wright, R. Saha, and W.D. Nix: Deformation mechanisms of the $Zr_{40}Ti_{14}Ni_{10}Cu_{12}Be_{24}$ bulk metallic glass. *Mater. Trans. JIM* **42,** 642 (2001).
35. Z.F. Zhang, G. He, J. Eckert, and L. Schultz: Fracture mechanisms in bulk metallic glassy materials. *Phys. Rev. Lett.* **91,** 045505 (2003).
36. H. Li, A. Ghosh, Y.H. Hom, and R.C. Brandt: The frictional component of the indentation size effect in low load microhardness testing. *J. Mater. Res.* **8,** 1028 (1993).
37. M. Legros, B.R. Elliott, M.N. Rittner, J.R. Weertman, and K.J. Hemker: Microsample tensile testing of nanocrystalline metals. *Philos. Mag.* **A80,** 1017 (2000).
38. B.R. Lawn: *Fracture of Brittle Solids* (Cambridge University Press, Cambridge, U.K., 1993).